Metabolic modeling of microbial communities in the chicken ceca reveals a landscape of competition and co-operation

Irina Utkina[1,2], Yi Fan[3], Benjamin P. Willing[3], and John Parkinson[1,2,4,*]

[1] Department of Molecular Genetics, University of Toronto, Toronto ON, Canada

[2] Program in Molecular Medicine, Hospital for Sick Children, Toronto ON, Canada

[3] Department of Agricultural, Food and Nutritional Science, University of Alberta, Edmonton, Canada.

[4] Department of Biochemistry, University of Toronto, Toronto ON, Canada.

* To whom correspondence should be addressed.
jparkin@sickkids.ca

Keywords: metabolic modeling, keystone species, community assembly, poultry microbiome, cross-feeding

ABSTRACT

With their ability to degrade dietary fibers to liberate otherwise unavailable substrates, members of the Bacteroidales exert a substantial influence on the microbiome of the lower intestine. Currently our knowledge of how this influence translates to the metabolic interactions that support community structure is limited. Here we applied constraints-based modeling to chicken cecal communities to investigate metabolic interactions in the presence and absence of *Bacteroides*. From metagenomic datasets previously generated from 30 chicken ceca, we constructed 233 metagenome-assembled genomes. Metabolic modeling of communities built from these genomes generated profiles of short chain fatty acids largely consistent with experimental assays and confirmed the role of *B. fragilis* as a metabolic hub, central to the production of metabolites consumed by other taxa. In its absence, communities undergo significant functional reconfiguration, with metabolic roles typically fulfilled by *B. fragilis* assumed by multiple taxa. Beyond *B. fragilis*, we found *Escherichia coli* and *Lactobacillus crispatus* also mediate influential metabolic roles that vary in the presence or absence of *B. fragilis*. Compensatory adaptations adopted by the microbiome in the absence of *B. fragilis* resulted in metabolic profiles previously associated with inflammatory bowel disease in humans, including energy deficiency, increased lactate production and altered amino acid metabolism. This work demonstrates the potential of chicken cecal microbiomes to investigate the complex metabolic interactions and key contributions that drive community dynamics.

INTRODUCTION

The gut microbiome consists of a complex, yet stable, community of microbes that confer beneficial roles to their host including the extraction of key nutrients, promoting gut health and limiting colonization by pathogens. Helping organize these communities are metabolic interactions involving the sharing (cross-feeding) of metabolites between taxa[1]. Many of these interactions are thought to be mediated by so-called keystone taxa which play a crucial role in shaping microbial community structure and function[2–7]. Within gut communities, keystone taxa are represented by genera such as *Bacteroides* and *Lactobacillus* that have been shown to exert considerable influence within their communities[8,9]. For example, while *Bacteroides* spp. play an important role in the degradation of complex carbohydrates and production of short chain fatty acids (SCFAs)[10,11], *Lactobacillus* spp. have been identified as divisive members, characterized by both positive and negative interactions with other microbes[12]. Currently our understanding of the cross-feeding relationships that drive community dynamics and the contribution of keystone taxa is limited.

Community metabolic modeling offers a powerful approach to unravel the complex interactions within the gut microbiome. Integration of genome-scale metabolic models from multiple microbes within a community-scale framework provides a mechanistic basis to dissect the metabolic landscape of microbial communities and the contributions of individual taxa[13–15]. Recent advances in community-scale metabolic modeling have enabled predictions of the production of key metabolites such as SCFAs, which help support gut health[16,17] as well as identification of potential cross-feeding interactions between bacterial species[13–15] and changes in the concentrations of metabolites associated with a variety of human diseases[18,19]. Beyond human health, the gut microbiome has attracted considerable interest from the livestock industry. For example, with global bans on the use of antibiotic growth promoters (AGPs)[20] attention is turning to manipulating gut communities in chickens to address issues of food insecurity associated with a surge in enteric infections[20].

In this study, we leverage community metabolic modeling to investigate the influence of keystone taxa on microbial communities associated with the chicken cecum, a major site of digestion of insoluble fibers and fermentation and host to the most diverse community in the poultry gut.

Applying *in silico* modelling based on previously published metagenomic data, we investigate the impact of *Bacteroides fragilis* on community and metabolic dynamics. Our models reveal that *B. fragilis* significantly impacts microbial diversity and structure of metabolic interactions. In *Bacteroides*-depleted communities, we observe an increase in the influence of other taxa including *Escherichia coli*, *Anaerostipes butyraticus*, and *Lactobacillus crispatus,* leading to a functional reorganization of the microbiome. Our findings highlight the pivotal role of the unique metabolic capabilities of *B. fragilis* and the potential implications for host health and productivity in its absence.

75 # RESULTS

76 **Bacteroides species influence the microbiome composition and functional capacity**

77 To examine the metabolic influence of keystone taxa within cecal microbial communities we
78 divided 33 samples from a recent study of 7-day old chickens[11] into two groups: one characterized
79 by the presence of *Bacteroides* species (HB, n=15), specifically *B. fragilis*, and the other without
80 *Bacteroides* species (NB, n=18)[11]. Metagenomic datasets previously generated from these samples
81 were used to generate metagenome-assembled genomes (MAGs). To enhance MAG quality and
82 consistency across samples, we conducted both individual assemblies for each sample and a co-
83 assembly of all samples. This combined approach allowed us to capture species present in
84 individual samples and improve assembly quality for shared taxa by leveraging the combined data.
85 Additionally, we re-assembled common taxa by pooling the corresponding reads from multiple
86 samples (see Methods). This process yielded 237 high- and medium-quality MAGs (defined as
87 having ≥50% completeness and ≤10% contamination) representing 227 taxa. Each MAG
88 represented at least 0.5% relative abundance in at least one of the 33 samples (**Figure 1A**).
89 Communities were largely dominated by representatives of families such as Lachnospiraceae,
90 UBA660, and taxa belonging to Oscillospirales order, with significant variations in their relative
91 abundances across samples (**Figure S1**). Next, we generated genome-scale metabolic models for
92 each MAG, refining models through gap-filling and manual curation to ensure their ability to
93 support growth on a corn feed diet and incorporate missing carbohydrate-active enzymes and
94 fermentation pathways (see Methods). Subsequently, models were combined to reflect the cecal
95 samples from which they were derived resulting in communities represented by 5 to 33 taxa with
96 an average of 1,096±98 unique enzymes (as defined by enzyme commission numbers; ECs; **Figure**
97 **1A**). Further, each community contained from 2,187 to 3,368 (mean 3,001±280) unique reactions
98 encompassing from 143 to 598 (mean 495±83) unique pathways (defined in MetaCyc[21]), with the
99 number of unique pathways being significantly higher in NB communities compared to HB
100 (p=0.0045, Wilcoxon Rank-Sum test; **Figure 1B**).
101
102 Our reconstructed metabolic models revealed distinct metabolic profiles among taxa. *E. coli* had
103 the largest number of enzymes, with broad representation across all pathways suggesting high
104 functional diversity (**Figure S2; Table S1**), although we acknowledge this may also reflect its well

annotated genome. *Bacteroides*, *Alistipes*, *Helicobacter*, *Barnesiella*, and *Coprobacter* spp., found exclusively in HB communities, exhibited expanded functionality in glycan and vitamin metabolism, suggesting they may play a dominant role in the breakdown of dietary fibers and vitamin synthesis. While most taxa possessed core functionalities across the major pathways, species within UBA1242 (e.g., *Caccovivens* spp.), UBA660 (e.g., *Faecenecus* and *Faecimonas* spp.), and CAG-508 (e.g., *Merdicola* spp.) families displayed sparser coverage of functions within carbohydrate metabolism. These microbial groups have been recently identified in diverse animal and human gut environments and are characterized by limited metabolic capabilities[22–27]. Despite their distant phylogenetic relationships, they each exhibit reduced genome sizes, diminished genetic repertoires, and numerous auxotrophies[28,29]. Further, these taxa exhibited minimal overlap with other species in amino acid metabolism capabilities, with distinct sets of enzymes involved in amino acid metabolism and xenobiotic biodegradation, suggesting they occupy a unique niche (e.g. mitigating environmental stressors) within the gut microbiome (**Figure S2**).

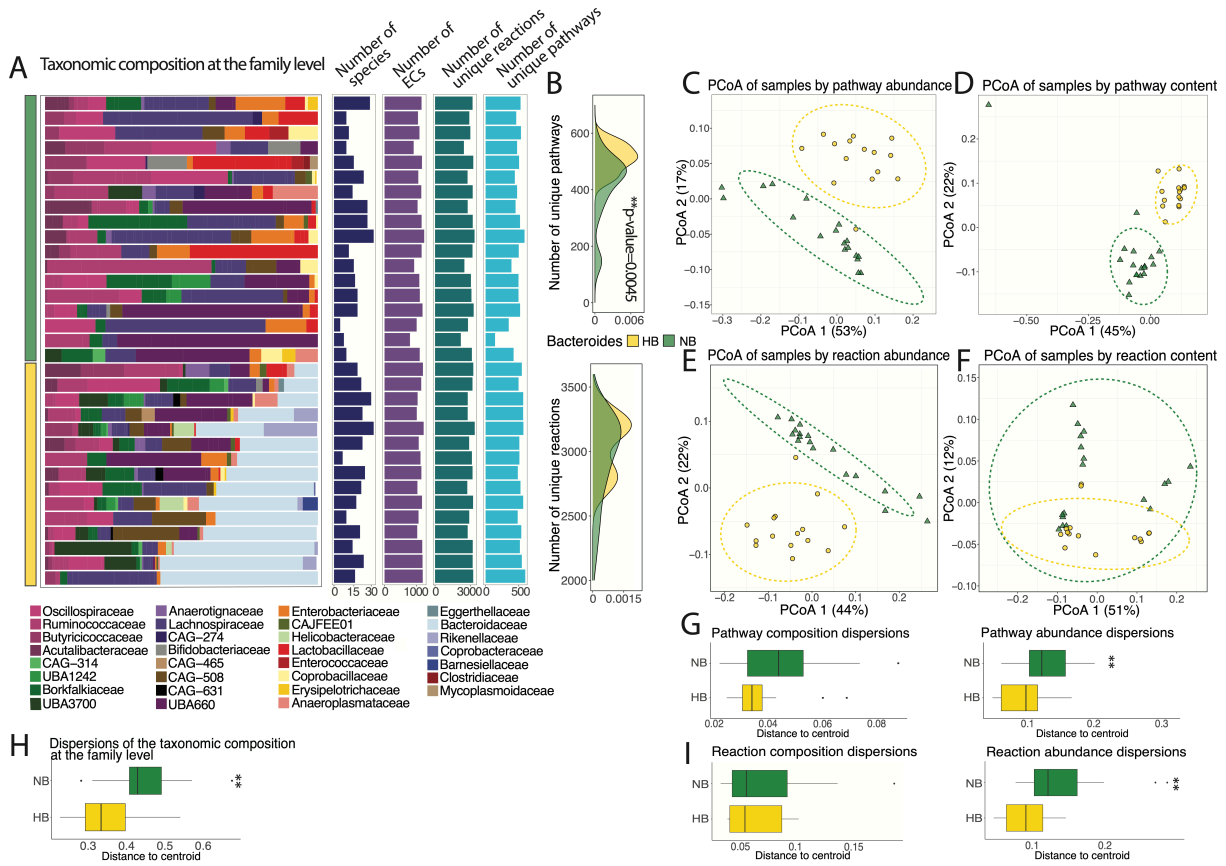

Figure 1. Taxonomic composition and functional analysis of chicken cecal microbial communities. A. Relative abundances of metagenome-assembled genomes (MAGs) consolidated by taxonomic family across 33 chicken cecal samples. The bar plots represent the numbers of

121 unique species, ECs, unique reactions, and unique pathways based on metabolic model's content.
122 Samples are categorized into two groups: those with high Bacteroides abundance (HB, gold) and
123 those without Bacteroides (NB, green). **B**. Distribution of numbers of unique metabolic reactions
124 and pathways in NB and HB samples. Significance determined using Wilcoxon rank-sum test. **C,**
125 **E**. PCoA of samples based on abundances of pathways (**C**) or reactions (**E**) content (i.e., reaction
126 and pathway counts within each sample were summarized by weighing them by the relative
127 abundance of the species contributing to that reaction or pathway), with dissimilarity matrices
128 calculated using the Bray-Curtis index. **D, F**. PCoA of samples based on the presence or absence
129 of pathways (**D**) or reactions (**F**) using Jaccard distances.
130

131 Interestingly, while the prevalence of *Lactobacillus crispatus, Anaerostipes butyraticus* and *E. coli*
132 in NB samples suggests that these taxa may become more dominant in the absence of *B. fragilis*,
133 members of UBA660 family, specifically, *Faecenecus gallistercoris* and *Faecimonas*
134 *intestinavium*, exhibit relatively high abundance (15-68%) in samples where the former three taxa
135 are absent or exhibit low abundance (**Figure S1**). This may indicate competitive relationships,
136 where less metabolically versatile taxa exploit specific substrates or metabolic niches that are less
137 accessible to other bacteria. Members of the Oscillospirales order exhibited enhanced functionality
138 in the metabolism of cofactors and vitamins, as well as carbohydrate metabolism, aligning with
139 their roles in fiber degradation and SCFA production (**Figure S2**). These diverse metabolic
140 capacities and interdependent roles of bacteria in the chicken cecal microbiome illustrate the
141 complex relationships driving microbial community structure.
142

143 Principal Coordinate Analysis revealed that the presence of *B. fragilis* significantly influences both
144 the taxonomic composition and metabolic potential of microbial communities (**Figures 1C-F**). NB
145 and HB samples segregate on the basis of reaction and pathway content, regardless of similarity
146 metric used. The high percentage of variance explained by the first two principal coordinates (70%
147 for Bray-Curtis dissimilarity based on pathway abundance and 67% for Jaccard distance) together
148 with a significant difference in metabolic pathway profiles (PERMANOVA p=0.001) highlights
149 the impact of *B. fragilis* on community metabolism. However, the differences in within-group
150 variability are not significant (TukeyHSD test p=0.13, permutest p=0.11) between the HB and NB
151 groups (**Figure S3C**). Moreover, we observed distinct pathway and reaction abundance profiles
152 between HB and NB groups (PERMANOVA p=0.001 for both), with greater variability within the
153 NB communities (TukeyHSD p=0.015 and p=0.006, permutest p=0.009 and p=0.004, for

154 pathways and reactions, respectively; **Figure S3B-C**). Overall, these findings show that *B. fragilis*
155 has a major influence on metabolic interactions within the gut microbiome.

156 **Community metabolic modeling accurately predicts the production of acetate and**
157 **propionate**

158 To further dissect the metabolic contributions of *B. fragilis* within their communities we
159 constructed *in silico* models for each of the 33 samples using the BacArena framework[30] in which
160 the relative abundance of each taxon was defined from the metagenomic datasets. Our *in silico*
161 model was designed to mimic the physiochemical conditions of the chicken cecum, including low
162 oxygen, neutral pH, peristalsis and release of cecal contents[29–32](see Methods). To assess the
163 accuracy of our *in silico* ceca models, simulations were performed for 16 hours (representing a
164 cycle of feeding), and predicted SCFA concentrations were compared with those previously
165 measured experimentally[11]. We found a significant correlation between the predicted and
166 experimentally derived concentrations for both acetate (spearman rho=0.53, p-value=0.0015;
167 **Figure 2A**) and propionate (spearman rho=0.52, p-value=0.0021; **Figure 2A**). Moreover, the
168 simulations reflected the experimentally measured differences for the NB and HB communities,
169 although we note the model over-predicted the production of propionate by *Bacteroides* species
170 (**Figure 2B**, **Figure S4**). The model was less predictive of butyrate production, potentially as a
171 result of the model missing the impact of host epithelial cells which are known to uptake
172 microbially derived butyrate[31,32]. Further, the discrepancy in the prediction of butyrate flux arises
173 from the presence of butyrate-producing organisms (e.g. *Butyricicoccus* and *Faecalibacterium*
174 spp.) in samples where the measured concentration was nearly zero. Previous studies have
175 demonstrated cross-feeding interactions between *Bifidobacterium* spp. and *Faecalibacterium* spp.,
176 with acetate produced by the former enhancing butyrate production in the latter[33]. In our
177 simulations, acetate produced by *Bifidobacterium pullorum* was utilized by other taxa, including
178 *Butyricicoccus* and *Faecalibacterium* spp.[34–36], to generate butyrate (**Figure S4**). This highlights
179 the importance of studying metabolic interdependencies to better understand SCFA production in
180 the gut microbiome. Overall, our models were able to accurately capture general trends and known
181 dynamics of SCFA production, correctly predicting interactions between key gut microbes.
182
183

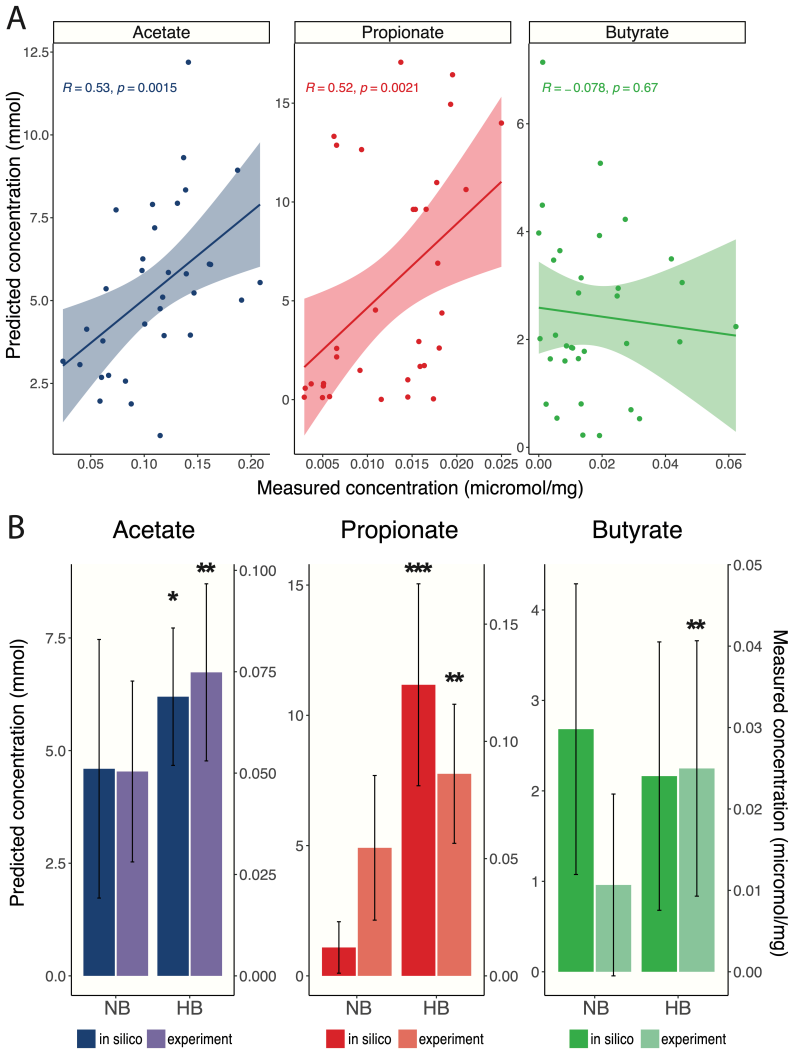

Figure 2. **Comparison of predicted and measured SCFA concentrations in chicken cecal samples. A**. Spearman rank correlation between *in silico* predicted and experimentally measured concentrations of acetate, propionate, and butyrate, with correlation coefficients (Spearman rho) and p-values indicated for each SCFA. Lines are fitted linear regressions, and colored areas around them indicate the 95% confidence interval. Each data point represents a sample. **B**. Bar plots comparing the average predicted and measured SCFA concentrations in samples with no Bacteroides (NB) and high (HB) Bacteroides abundance. The plots indicate the mean concentrations and standard errors for acetate, propionate, and butyrate with asterisks corresponding to the significance levels (Wilcoxon Rank-Sum test): * - p-value < 0.05, ** - p-value <0.01, *** - p-value < 0.001.

E. coli and *B. fragilis* drive metabolic dynamics in the chicken cecal microbiome

Our analysis of metabolic interactions within chicken cecal microbial communities revealed distinct structural differences between HB and NB communities. To further investigate these differences, we used mutual information (MI) scores to construct a network based on metabolic

198 overlap, where metabolic similarity refers to the extent of shared metabolic reactions between
199 communities. We found that NB communities exhibited higher metabolic similarity than HB
200 communities (pairwise MI scores 0.134±0.076 for NB and 0.123±0.068 for HB; **Figure 3A**).
201 Although the difference in MI scores between NB and HB communities was not statistically
202 significant (p=0.065, Wilcoxon Rank-Sum test), the trend suggests that the absence of *B. fragilis*
203 leads to greater metabolic similarity. Since *Bacteroides* spp. play a fundamental role as primary
204 fermenters and are often considered keystone taxa in their communities[37–40], their potential
205 monopoly of key resources may drive the reduction in community interactions and metabolic
206 diversity. Moreover, the presence of both *B. fragilis* and *E. coli* resulted in further
207 compartmentalization of metabolic functions, as evidenced by significantly lower overlap in
208 metabolic functions (MI score 0.128±0.061) compared to NB communities with *E. coli* (MI score
209 0.154±0.08; p=0.022, Wilcoxon Rank-Sum test) and without *E. coli* (MI score 0.21±0.11; p=1e-
210 05, Wilcoxon Rank-Sum test) (**Figure 3A)**. Interestingly, samples lacking *E. coli* species exhibited
211 highest pairwise MI scores (0.213±0.111 and 0.21±0.11, for HB and NB communities
212 respectively**)** indicating that absence of *E. coli* promotes higher metabolic similarity irrespective
213 of the presence or absence of *B. fragilis.* These findings suggest that consistent with its wide range
214 of metabolic functions, *E. coli* acts as a metabolic generalist – a species capable of performing a
215 broad range of metabolic activities, in contrast to specialists that have more limited, niche-specific
216 roles – to fulfill roles vacated by other keystone taxa to support the metabolic versatility of the
217 cecal microbiome (**Figure S2; Table S1**).
218
219 While MI scores did not show a significant difference in metabolic similarity in NB and HB
220 communities, the influence of additional taxa such as *E. coli* led us to investigate whether the
221 absence of *B. fragilis* results in communities exhibiting a greater diversity of less dominant taxa,
222 with increased competition and metabolic interactions. We applied three complementary metrics
223 (see Methods): Metabolic Resource Overlap (MRO) score, a metric that quantifies both
224 competition for shared resources as well as complementarity in metabolic capabilities[41];
225 Community Metabolic Dissimilarity (CMD) score, a metric that quantifies the diversity of
226 metabolic functions in a community; and Cross-Feeding Coefficient (CFC) based on the number
227 of metabolite exchanges. We found that NB communities had significantly higher MRO (p=1.2e-
228 05, Wilcoxon Rank-Sum test) and CFC (p=0.025, Wilcoxon Rank-Sum test) scores than HB

communities (**Figure 3B-C**). While NB communities also featured higher CMD scores, consistent with reports showing that metabolic dissimilarities enhance cross-feeding between species[42], this difference was not significant. Overall, these findings show that NB communities exhibit greater metabolic similarity between communities, along with enhanced cross-feeding relationships and higher metabolic diversity within individual communities, supporting the hypothesis that the presence of *B. fragilis* reduces metabolic diversity and interactions.

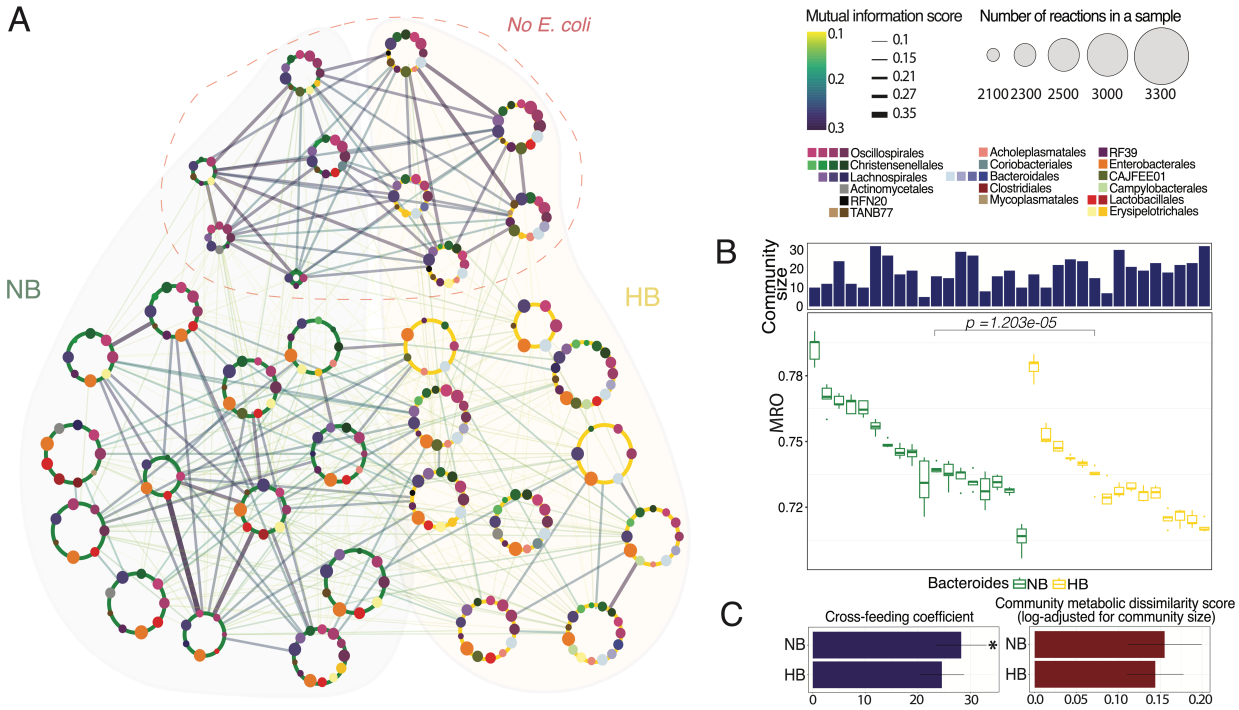

Figure 3. *E. coli* and *B. fragilis* influence metabolic similarity and cross-feeding in chicken cecal microbiomes. A. Mutual information-based network of chicken cecal microbial communities, highlighting metabolic similarities based on metabolic reaction content. Nodes represent samples, with sizes corresponding to the number of unique reactions in a sample, colored by category: no Bacteroides (NB, green) and high Bacteroides (HB, gold). Edges are colored and thickened according to the mutual information score, with thicker and darker edges indicating higher similarity. The top region outlined in red indicates samples lacking E. coli. Sizes of the smaller nodes within a sample correspond to the number of reactions covered by the metabolic models of species belonging to a respective taxonomic family (grouped by taxonomic order below). **B.** Bar plots showing community sizes (top) and box plots showing Metabolic Resource Overlap (MRO) within each sample (summarizing five *in silico* replicates). NB communities exhibit significantly higher MRO (p=1.203e-05, Wilcoxon Rank-Sum test) **C.** Cross-feeding coefficient (left) and Community Metabolic Dissimilarity (CMD) score (right) between NB and HB communities. NB communities show a significantly higher cross-feeding coefficient (*p=0.025) and a higher average CMD score.

250 **Functional reorganization and emergence of alternate hubs in response to the absence of**
251 **keystone taxa in the gut**

252 Building upon the finding that the presence or absence of *B. fragilis* influences cross-feeding
253 relationships among other taxa, we extended our analyses to examine changes in metabolite
254 exchange dynamics in a larger set of taxa that could be considered metabolic hubs (defined here
255 as taxa exchanging at least 12 metabolites with at least 10 other taxa across samples within each
256 category; 87 taxa total - 40, 22 and 25 taxa associated with NB only, HB only and both,
257 respectively). These taxa were used to generate profiles of interactions with other taxa and
258 subsequently clustered to identify cliques of cross-feeding taxa (**Figure 4A; Table S2**). Consistent
259 with our previous findings *B. fragilis* represents the central hub in the HB communities, while in
260 its absence, *E. coli, A. butyraticus* and *L. crispatus,* adopt a greater range of metabolic interactions.
261 The shift towards a more partitioned network observed in NB communities was further
262 characterized by the formation of distinct cliques, representing groups of taxa engaging in mutual
263 cross-feeding interactions. Within each clique, a single taxon (e.g. *Mediterraneibacter*
264 *sp904377845, Lactobacillus johnsonii* and *Borkfalkia sp944368795*) appears to dominate
265 interactions acting as a metabolic hub for each group of taxa.
266
267 To further clarify how 'metabolic hub' taxa exert their influence within their communities, we
268 examined their interactions with other taxa in the context of prevalence across samples, relative
269 abundance, and provision of unique functionality (**Figure 4B, Figure S5**). Surprisingly, a taxon's
270 unique metabolic potential within its community (as estimated by the number of unique enzymes)
271 did not correlate with its number of metabolic interactions (**Figure S5A**) although we did observe
272 a positive correlation with prevalence (**Figure S5B**). These findings suggest that while the number
273 of unique functions a taxon brings to a community might increase its ability to engraft, the
274 community does not exploit that additional functionality. Indeed, *E. coli*, which is both prevalent
275 and possesses the greatest set of unique functions, appears to benefit in its community from the
276 consumption of many metabolites from multiple species with only modest contributions to
277 production (**Figure 4B**). Other prevalent taxa exhibiting a broad range of interactions, such as *L.*
278 *crispatus* and *A. butyraticus,* with fewer unique enzymes did not exhibit the same disparity in
279 consumption and production. At the other end of the spectrum, we found some less prevalent taxa,
280 present in only a limited number of samples (e.g., *L. johnsonii* and *M. sp904377845*) exert their

influence by specializing in the production of a wide array of metabolites utilized by a large number of other taxa (**Figure 4B**).

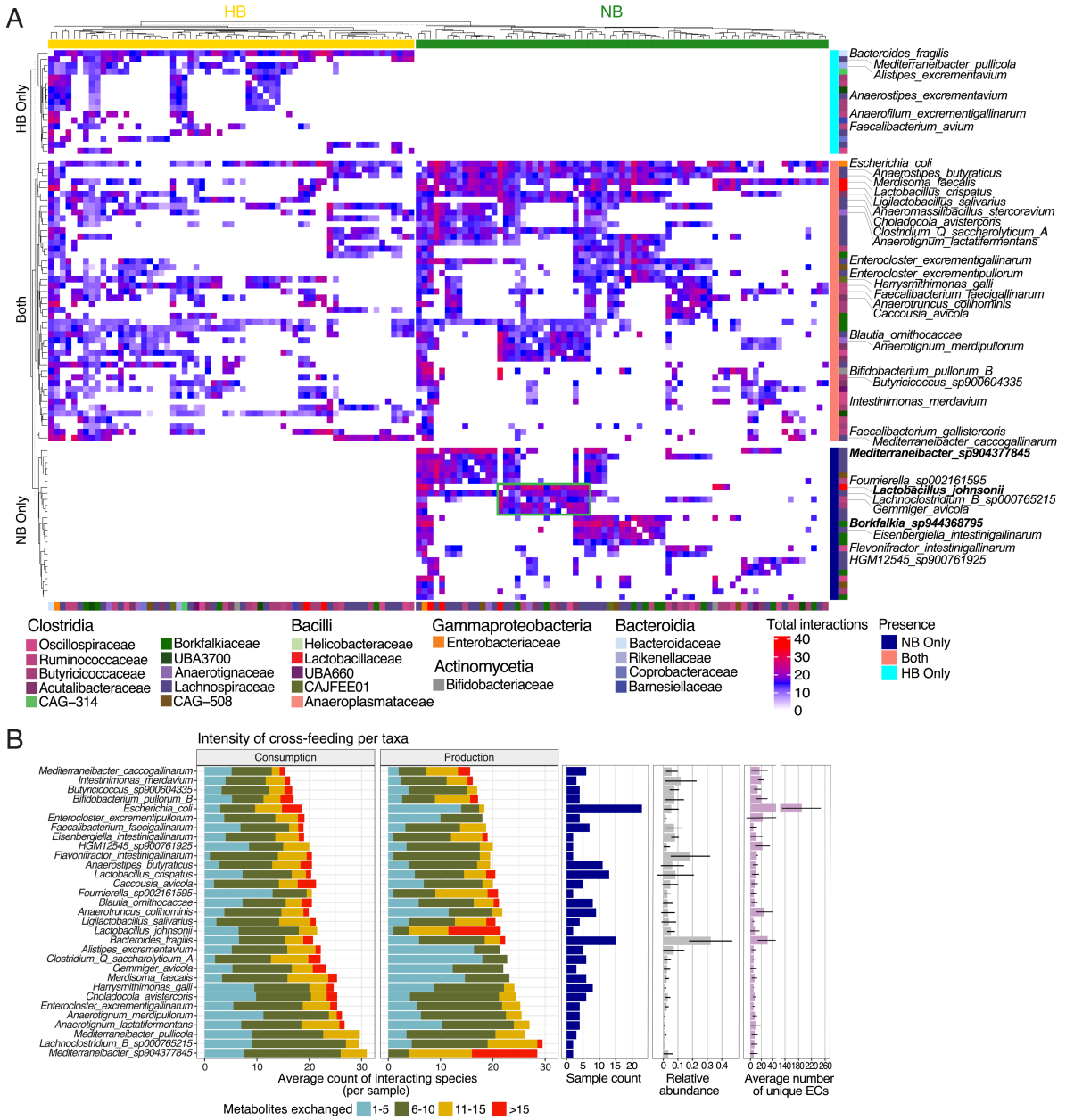

Figure 4. Major metabolic hubs and cross-feeding dynamics in HB and NB microbial communities. A. Heatmap of interactions between species, highlighting top cross-feeders defined as those forming at least 10 cross-feeding pairs with the exchange of a minimum of 12 metabolites across samples within each category, HB or NB. The interactions observed across multiple samples within each category were normalized by the number of samples in which each cross-feeding pair was present. Key taxa are labeled in this heatmap, including taxa present in at least two samples, forming an average of at least 230 interactions per sample and possessing on average at least 5 unique EC per sample. The tiles in the heatmap are colored based on the normalized total number of interactions for each species pair, with a color gradient indicating the interaction intensity.

Blocks of taxon interactions represent 'cliques', indicating groups of species with frequent metabolic exchanges. For example, the green-highlighted clique shows *Lactobacillus johnsonii* acting as a 'metabolic hub,' engaging in extensive interactions with taxa from the families Lachnospiraceae (*Lachnoclostridium B sp000765215*, *Fusicatenibacter sp900543115*, *Blautia ornithocaccae*, *Eisenbergiella sp904392525*, *Choladocola avistercoris*, *Merdisoma faecalis*), Acutalibacteriaceae (*Eubacterium R faecavium*, *Acutalibacter ornithocaccae*, *Anaeromassilibacillus stercoravium*), Borkfalkiaceae (*Coproplasma stercoravium*, *Coproplasma stercorigallinarum*), Anaerotignaceae (*Anaerotignum merdipullorum*), Butyricicoccaceae (*Butyricicoccus avicola*), Ruminococcaceae (*Gemmiger avicola*), and Oscillospiraceae (*Dysosmobacter pullicola*), as well as with each other. Taxa mentioned in the main text are highlighted in bold. **B**. Stacked bar charts representing the intensity of cross-feeding per taxon. The bars indicate the average number of interacting species for each taxon per sample, divided into metabolite consumption (left) and production (right). Colors correspond to the number of metabolites exchanged, with categories ranging from 1-5, 6-10, 11-15, and >15 metabolites. The bar plots to the right represent the sample count (number of samples in which each species is present, blue), relative abundance (grey), and the average number of unique enzymes (ECs) taxon possesses per sample (purple). Subset of taxa displayed is present in at least two samples, exhibit an average of at least 230 total interactions per sample, and possess a minimum of 5 unique EC numbers per sample.

These findings reveal a hierarchy of taxa acting as metabolic hubs, where taxa such as *B. fragilis* and *E. coli* are responsible for driving the bulk of interactions, supplemented by additional hubs like *A. butyraticus* and *L. crispatus*. Further, within their communities, there exist cliques of taxa sharing metabolic interactions, organized around relatively rare taxa. This hierarchy highlights the varying abilities of each type of hub taxa to colonize within their communities, with *B. fragilis* and *E. coli* capable of colonizing many communities and establishing extensive cross-feeding networks. Others such as *M. sp904377845* and *L. johnsonii*, appear more limited in their ability to colonize communities and feature a smaller range of interactions with only a subset of taxa.

Role of key metabolic hubs in modulating cross-feeding interactions

To further assess how the presence/absence of different metabolic hubs may impact cross-feeding relationships within their communities, we constructed a linear model based on the abundance of *E. coli* and the presence/absence of three additional metabolic hub taxa (*A. butyraticus, L. crispatus* and *B. fragilis*; see Methods). A relatively high abundance (>5%) of *E. coli* abundance was associated with increased cross-feeding in *Bacteroides*-depleted communities, potentially indicating the ability of *E. coli* to replace community functions otherwise performed by *B. fragilis* (**Figure S5C; Table S3**). Interestingly, only one of the 15 HB samples exhibited such an abundance, indicating competition between these two taxa. Extending this analysis to two other

329 metabolic hub taxa (*A. butyraticus* and *L. crispatus*), we found their presence in the absence of *E.*
330 *coli* was associated with increased cross-feeding activity, suggesting their ability to provide an
331 alternative source of metabolic functions (**Figure S5D-E; Table S3**). Communities featuring both
332 *E. coli* together with *A.butyraticus* displayed lower cross-feeding activity, reflecting potential
333 competition between these taxa. In contrast, NB communities with *L. crispatus* showed higher
334 cross-feeding activity compared to HB communities, regardless of *E. coli* abundance, indicating
335 an antagonistic relationship between *L. crispatus* and *Bacteroides*.
336
337 Since our linear model focused only on taxa representing metabolic hubs, we were interested in
338 how other metabolic hub taxa, specifically those mediating interactions within a subset of taxa
339 (cliques), contribute to their communities. To avoid the confounding influence of dietary
340 metabolites, we further restricted these analyses to metabolites only produced by bacteria. As
341 before, *B. fragilis* represents the central hub in the HB communities, while *E. coli, A. butyraticus*
342 *and L. crispatus* assume additional interactions in NB communities (**Figure S6A; Table S4**).
343 Moreover, we also observed the formation of metabolic cliques, with greater numbers of
344 interactions in NB communities. Comparing the eight largest cliques specific to either NB or HB
345 communities (labelled A-H), we identified 48 unique microbially-derived metabolites exchanged
346 within these cliques (ranging from 24 in clique H to 37 in clique A). While taxa associated with
347 these cliques may not necessarily be present in the same samples, these cliques nonetheless
348 represent groups of taxa that occupy a similar metabolic niche – that is, they share specific sets of
349 metabolic functions and interactions they engage in, contributing to similar ecological roles across
350 different communities.
351
352 This aligns with previous research demonstrating enrichment of mutualistic interactions in co-
353 occurring microbial communities[41]. While there is a substantial overlap in metabolites exchanged
354 across the eight cliques investigated – 17 metabolites were common to all cliques, and an additional
355 16 were shared among at least five cliques (**Figure S6B**) – individual cliques exhibit unique
356 metabolic exchanges reflecting the specific taxa involved. This suggest that, despite a shared core
357 of metabolic pathways and intermediates, each clique possesses distinct metabolic interactions
358 driven by its constituent taxa. For instance, in the NB-specific clique B, *Bifidobacterium* spp. And
359 members of Lactobacillaceae uniquely produced and exchanged D-alanine, melibiose, and

360 spermidine (**Figure S6A-B**). Relative to other cliques, clique D, comprising members of
361 Oscillospirales, Lachnospirales, Christensenellales, Coriobacteriales, and RF39, exhibited a more
362 limited range of metabolite exchanges, lacking common fermentation products but uniquely
363 exchanging NAD, highlighting the role of redox reactions and energy metabolism within this
364 clique. These findings highlight how specific taxa contribute to functional diversity within
365 microbial communities by occupying distinct metabolic niches, thereby shaping the overall
366 metabolic landscape of their environments.
367
368 The changes in cross-feeding relationships associated with the absence of *B. fragilis* led us to
369 investigate how this translates in terms of exchange of specific metabolites. We therefore analyzed
370 the production and consumption of 18 metabolites selected on the basis of their relationship with
371 4 keystone taxa (see Methods; **Figure 5**). As expected, in HB communities *B. fragilis* is the
372 predominant producer, contributing to the majority of the production of 10 metabolites, with *E.*
373 *coli, Mediterraneibacter glycyrrhizinilyticus, Faecalibacterium gallistercoris,* and
374 *Dysosmobacter pullicola* largely responsible for the production of a more limited set of metabolites
375 including methanol, indole, uridine, formate and L-glutamine. In NB communities, the production
376 of these metabolites is redistributed to multiple other species. For example, consistent with
377 previous reports[33,36,43,44], in the absence of *B. fragilis*, *E. coli* assumes the production of multiple
378 metabolites otherwise produced by *B. fragilis* including acetate (along with members of
379 *Clostridia*), ammonium (with *A. butyraticus*), succinate, propionate, sorbitol and GABA. These
380 activities are supported through the production of lactate, uridine and L-glutamine by *L. crispatus*,
381 the latter consistent with previous reports of its production[45]. In the presence of *B. fragilis*, *E. coli*
382 alters its metabolic contributions to the generation of methanol, itself utilized by *B. fragilis.*
383 Interestingly, in NB communities *A. butyraticus* adopts the role of methanol production (**Figure**
384 **5**).
385
386 Together our predictions show that in the absence of a keystone taxon (here *B. fragilis*), the cecal
387 microbial community undergoes significant reorganization, characterized by the emergence of
388 alternate metabolic hubs as well as a shift in metabolite production and consumption profiles by
389 taxa present in both types of communities.

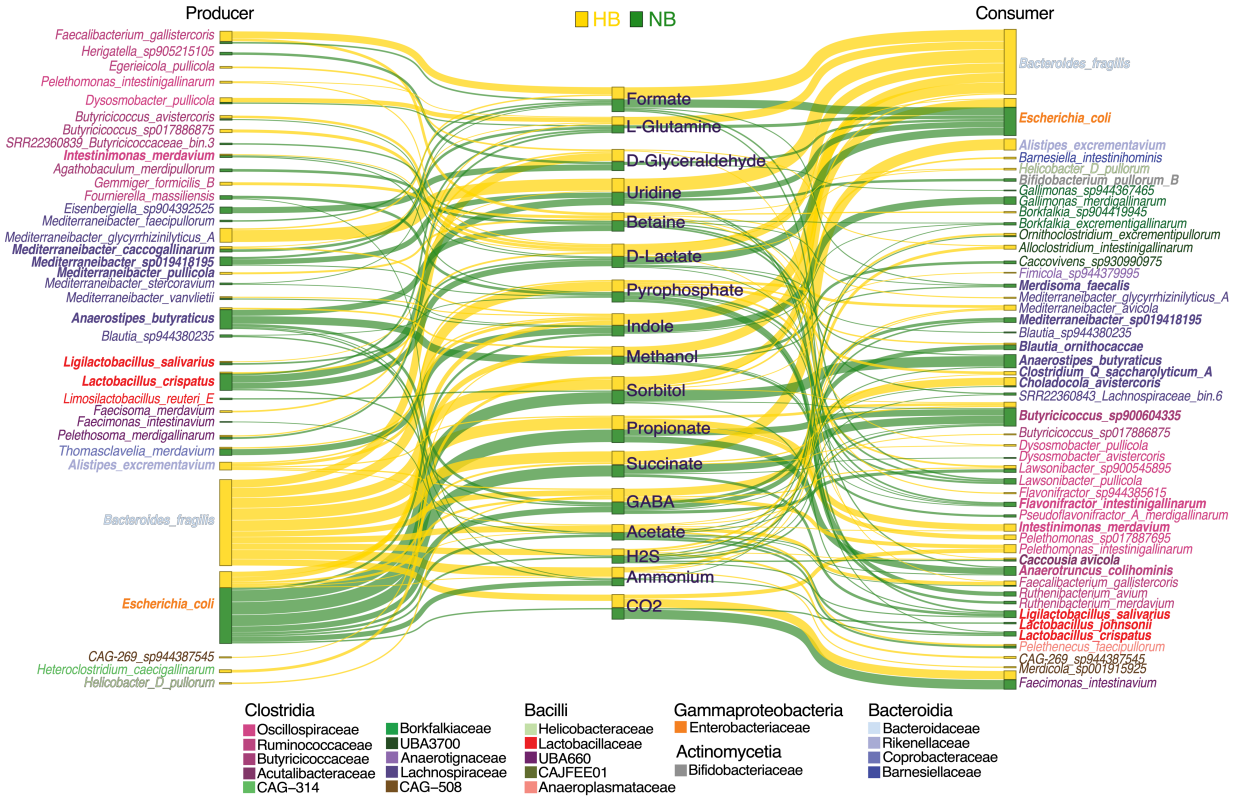

Figure 5. Shifts in cross-feeding networks: metabolic role redistribution in HB and NB communities. The Sankey diagram illustrates the cross-species interactions between primary producers and consumers of key cross-fed metabolites in the HB and NB communities. Producers are displayed on the left, cross-fed metabolites in the middle, and consumers on the right. Gold links represent contributions in HB communities, while green links represent those in NB communities. The thickness of each link is proportional to the contribution of the species (as a percentage) to the total production or consumption of each metabolite. To highlight the major players in cross-feeding dynamics, only the top three producers and consumers for each metabolite are shown, with a cutoff set at a minimum 5% contribution across samples within each category. Species highlighted in bold were previously described in Figure 4B. The diagram provides a visual summary of how key microbial taxa participate in the metabolic exchange, highlighting functional shifts between HB and NB communities.

Metabolic reorganization associated with the loss of *Bacteroides* in the chicken cecum reflects disease-associated metabolism in human IBD

Our comparisons of HB and NB communities, exhibit notable similarities to microbiome profiles associated with Inflammatory Bowel Disease (IBD) in humans (Ulcerative Colitis - UC and Crohn's Disease - CD). Previous studies have reported shifts in the abundance and roles of both *B. fragilis* and *E. coli* – major metabolic hubs in our cecal communities – that correlate with disease states. The former being associated with reduced abundance in IBD patients, while the latter is associated with increased abundance[46–50]. Additionally, we observed increased abundance of

410 *Alistipes* and *Faecalibacterium* species in HB samples (**Figure S1**), consistent with communities
411 associated with healthy individuals in contrast to IBD patients[49,51,52]. Similarities between our
412 study of HB and NB communities with healthy/IBD communities also extend to metabolic
413 profiles. For example, the heterolactic fermentation pathway associated with lactic acid bacteria is
414 more prevalent in NB communities, resulting in increased starch consumption and lactate
415 production (**Figure 6**), consistent with elevated lactate levels observed in IBD patients[53–55]. NB
416 communities are also associated with reduced production of propionate, a key source of energy for
417 gut epithelial cells and a hallmark of IBD[55–58]. While studies have reported varied metabolic
418 profiles in IBD, with both increased and decreased energy metabolism[55,59–61], our findings align
419 with the broader trend of altered energy metabolism in disease state. Specifically, we observed a
420 metabolic shift in *Bacteroides*-depleted communities characterized by increased consumption of
421 coenzyme A (CoA) and glycerol, alongside increased production of TCA cycle intermediates such
422 as 2-oxoglutarate and citrate, as well as GTP. CoA, essential for fatty acid metabolism and the
423 TCA cycle as an acyl group carrier, is being consumed more by the microbial community,
424 suggesting upregulated lipid and energy metabolism pathways. However, the concurrent
425 accumulation of TCA intermediates may indicate a bottleneck or dysregulation within the
426 microbial TCA cycle, potentially due to limited CoA availability. This imbalance could reflect a
427 shift towards fermentative metabolism in the absence of B. *fragilis*. Notably, reduced CoA levels
428 have been observed in the colonic tissues of pig models and human patients with ulcerative colitis
429 (UC), where they are associated with impaired fatty acid oxidation and energy metabolism in host
430 cells[55,62]. While our findings pertain to increased microbial consumption of CoA, this could
431 potentially decrease its availability in the gut lumen, impacting the host's energy metabolism.
432
433 Beyond changes in energy metabolism, our models also predict an increase in production of amino
434 acids, including L-phenylalanine, L-valine and L-lysine in NB communities relative to HB (**Figure**
435 **6**), consistent with recent studies reporting alterations in levels of these amino acids in IBD
436 patients[53,57,63,64]. Other notable metabolic similarities include reduced profiles of 5-Methylthio-D-
437 ribose, a metabolite involved in the methionine salvage pathway, in NB communities, indicative
438 of reduced sulfur cycle activity and consistent with deficiencies in sulfur-containing metabolites
439 in microbial communities of IBD patients[18,19]. Thiamin, typically deficient in CD patients[53,65], is
440 predominantly produced by *B. fragilis*, and consequently reduced in NB communities. Finally, the

441 increased consumption of sialic acid (Neu5Ac), a mucin-derived monosaccharide, by NB
442 microbiomes suggests enhanced sialidase activity, which has been linked to intestinal
443 inflammation and provides a growth advantage to bacteria like *E. coli*[66,67]. Thus, while the earlier
444 study reported reduced inflammation in HB chicken cecal microbiomes[11], the opposite may be
445 inferred for NB microbiomes.

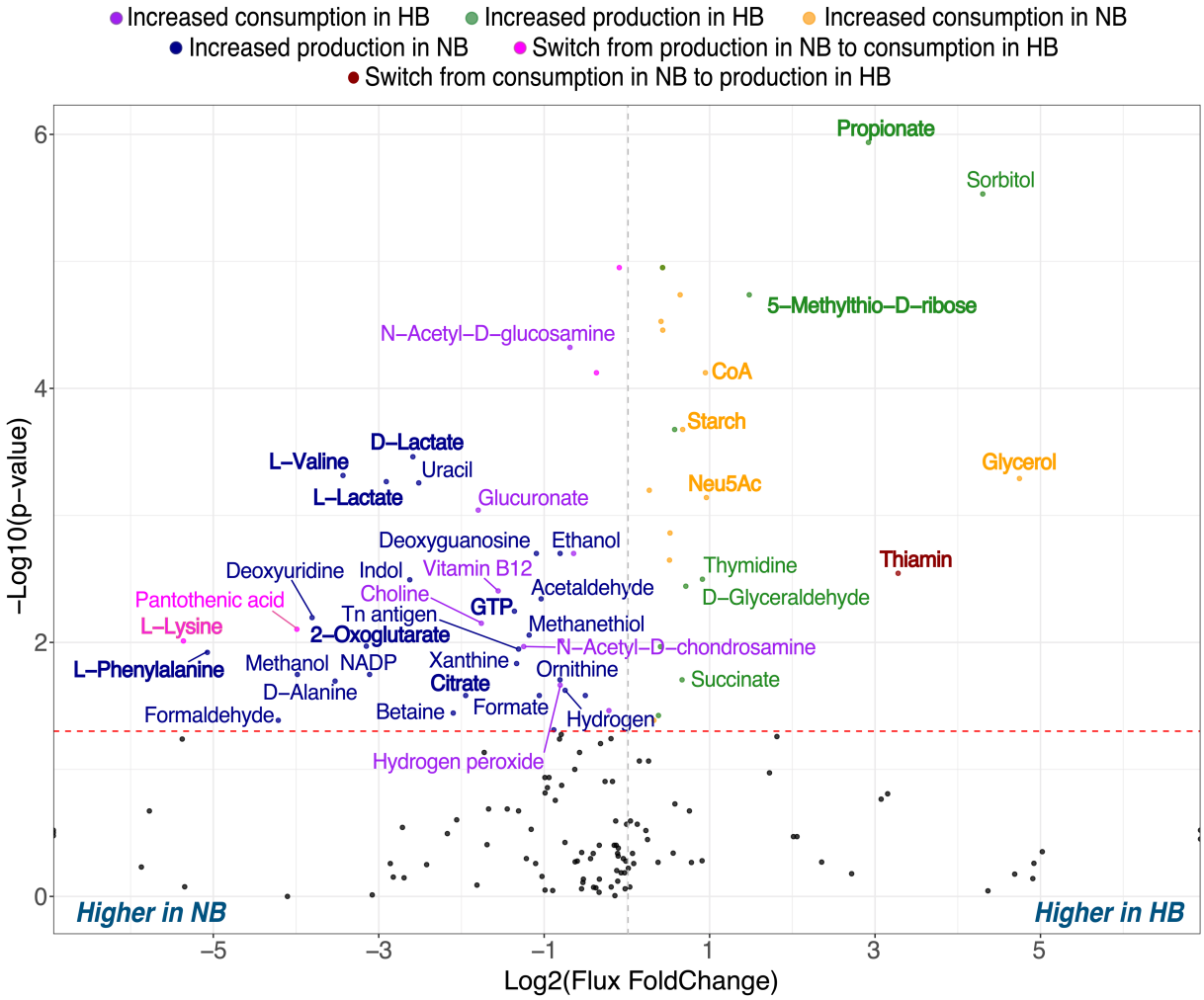

446 **Figure 6. Comparison of metabolite exchange patterns between HB and NB communities**.
447 Each dot represents a metabolite being exchanged, with black dots indicating metabolites that do
448 not show statistically significant changes in production or consumption between NB and HB
449 groups. Statistically significant differences in total community fluxes (normalized to community
450 size) were identified using the Wilcoxon rank-sum test. Dashed red line indicates the threshold for
451 significance level, p-value < 0.05. Metabolites are color-coded based on the direction of their
452 exchange: green - increased consumption in HB; blue - increased production in HB; orange -
453 increased consumption in LB; purple - increased production in LB; red - switch from production
454 in LB to consumption in HB; pink - switch from consumption in LB to production in HB.
455 Metabolites with an absolute log2FoldChange greater than 0.7 are labeled and colored accordingly;
456 metabolites discussed in results are highlighted in bold.
457

458 Overall, our findings reveal parallels between the community and metabolic dynamics of chicken
459 cecal communities in the absence of *B. fragilis* and those associated with IBD, suggesting
460 *Bacteroides*-rich communities may confer a protective role against inflammation.

461 **DISCUSSION**

462 Previous studies suggest microbial communities in the gut display a hierarchical structure, with
463 so-called keystone taxa acting as influential members through their ability to provide their
464 communities with unique metabolic capacities[7,68–70]. The Bacteroidaceae family members are
465 considered to be one of the most influential taxa, exerting a significant impact on metabolic
466 interactions withinn their communities[37–39,71,72]. Previous studies have shown that poultry gut,
467 specifically the cecum, exhibits substantial fluctuations in the abundance of members of the
468 Bacteroidaceae family, including the genus *Bacteroides*[11,73,74]. Notably, *Bacteroides* spp. are less
469 abundant in intensively raised chickens compared to those raised in extensive systems (i.e. with
470 access to the outdoors)[75]. Shifts in the abundance of *Bacteroides* can impact the community
471 dynamics resulting in reduced feed efficiency, and heightened susceptibility to enteric diseases[76–
472 78]. In humans, such shifts have also been associated with IBD[79,80].
473
474 Here we leveraged a pre-existing dataset of metagenomic data from the cecal communities of
475 chickens displaying a range of *Bacteroides* abundance and performed community metabolic
476 modelling to dissect the influence of keystone taxa on metabolic interactions within their
477 communities. Notably we found that our sample-specific community models accurately predicted
478 the production SCFAs, particularly acetate and propionate, and recapitulated experimentally
479 observed differences between *Bacteroides*-rich (HB) and -depleted communities (NB). Our
480 findings demonstrate that the absence of *B. fragilis* results in more similar metabolic profiles across
481 different microbiomes, while simultaneously increasing the range of metabolic functions within
482 each individual community. However, this shift does not necessarily lead to an increase in overall
483 microbial diversity. Moreover, NB communities exhibited significantly higher metabolic resource
484 overlap within communities and increased cross-feeding interactions. This trend aligns with the
485 role of *Bacteroides* spp. as keystone taxa, which typically dominate and monopolize key metabolic
486 functions, thereby reducing metabolic diversity within their communities[81,82].
487

488 By defining metabolic hubs as microbial taxa with a central role in metabolite exchange and
489 distribution, we examined their influence on the overall metabolic landscape. While *B. fragilis* acts
490 as a central hub, its absence triggers a shift towards a decentralized network characterized by
491 distinct cross-feeding cliques and the emergence of new metabolic hubs, such as *E. coli*, *A.*
492 *butyraticus*, and *L. crispatus*. Contrary to the expectation that a larger enzymatic repertoire directly
493 translates to greater community influence, we observed a diverse range of strategies, from
494 generalists like *E. coli,* which can perform a broad range of metabolic activities, to specialists like
495 *L. johnsonii,* which focus on specific metabolic functions**.** Our analyses show that *E. coli* has a
496 significant impact on cross-feeding, with increased activity when *E. coli* abundance exceeds 5%
497 in *Bacteroides*-depleted communities. Interestingly, *L. johnsonii* and *L. crispatus,* previously
498 described as eliciting a Marmite effect on the gut microbiome[12], emerged as alternative metabolic
499 hubs in the absence of *Bacteroides*, reflecting the antagonistic relationship between *Lactobacilli*
500 and *Bacteroides* a observed in previous studies[11,83–85]. While *L. crispatus* had a positive effect on
501 cross-feeding in the absence of *E. coli*, its presence in samples where *E. coli* was abundant led to
502 a decrease in metabolic interactions. These observations highlight the shifting role of *L. crispatus*
503 as it can both contribute to and limit the community's metabolic interactions, depending on the
504 presence of keystone taxa (e.g. *E. coli* and *B. fragilis*).
505
506 In our study we found *B. fragilis* plays a central role in the production of metabolites utilized by
507 other taxa whereas NB communities were characterized by a greater distribution of metabolic
508 functions across a broader range of taxa. While this might be expected to contribute to community
509 stability, similar changes in distributions are thought to contribute to disease associated with the
510 human gut[86,87]. Indeed, our comparative analysis of HB and NB communities revealed striking
511 parallels with IBD-affected human gut; NB communities exhibit increased lactate production,
512 energy deficiency, and altered amino acid metabolism, alongside increased markers of
513 inflammation. In contrast, HB communities displayed metabolic signatures associated with a
514 healthy gut state including a higher production of SCFAs and essential vitamins, such as thiamin.
515 Further, consistent with our cecal models, a decreased abundance of *Bacteroides*, particularly *B.*
516 *fragilis*, which are typically abundant in healthy individuals, has been observed in patients with
517 IBD, allowing opportunistic pathogens such as *E. coli* to flourish[46–50]. These findings highlight the

518 potential of using models of chicken cecal communities to study gut microbial ecology and disease
519 mechanisms.
520
521 This work establishes a framework for utilizing community metabolic modeling to study the
522 poultry gut microbiome. Our approach facilitates the prediction of metabolic outputs, such as
523 SCFA production, as well as elucidation of cross-feeding relationships. Moreover, our framework
524 offers a mechanistic understanding of how keystone taxa, like *Bacteroides,* influence the
525 ecological dynamics and metabolic landscape of the gut microbiome. Despite its promising results,
526 we acknowledge our platform is not without some limitations. For example, community-level
527 metabolic models may risk overemphasizing the metabolic roles of well characterized taxa, such
528 as *E. coli*[88,89]. Further, the absence of host-microbiota interactions ignore the potential contribution
529 of the host in terms of uptake of metabolites, as well as the influence of the host immune system.
530 While the models accurately predict overall trends in metabolite production, they may
531 overestimate or underestimate specific metabolic fluxes. This can be attributed to limitations in
532 the functionality of some bacterial models, influenced in turn by the quality of the corresponding
533 MAGs. Finally, the lack of data from upstream gut compartments may also limit our understanding
534 of the precise metabolic environment in the cecum; here we assume that dietary components in
535 amounts adjusted for known estimates of upstream absorption are directly available to members
536 of the cecal community, ignoring the potential metabolic contributions from microbes present
537 upstream of the ceca. Future research could integrate host factors, explore other gut regions, and
538 assess the potential for targeted interventions to beneficially manipulate the microbiome.
539

540 MATERIALS AND METHODS

541 External data collection

542 The experimental methods and data collection procedures have been described previously[11].
543 Publicly available raw sequence data and associated metadata associated with the study were
544 downloaded from the sequence read archive (SRA).

545 **Chicken cecal metagenomic samples analysis**

546 Metagenomic reads were subjected to quality filtering using BBTools/BBMap (v39.03)[90]. Single-
547 sample assemblies and co-assemblies of short reads were conducted with MEGAHIT (v1.2.9)[91],
548 specifying a minimum contig length parameter of '–min-contig-len' set to 1000. The Bowtie2
549 (v2.2.3)[92] tool was employed to index assemblies and map filtered reads onto the contigs, creating
550 abundance profiles. Following this, the metagenome assemblies underwent separate binning
551 processes utilizing MetaBAT2 (v2.13)[93] and CONCOCT (v1.1.0)[94]. Initially, samtools (v1.9)[95]
552 sorted the read mappings, and the read coverage was determined using the MetaBAT2 script
553 'jgi_summarize_bam_contig_depths'. Subsequently, the binning process involved the 'metabat2'
554 command with default settings for each assembly, using contig coverage across samples as input.
555 For CONCOCT, accessory scripts were employed to cut contigs into 10 kb fragments
556 (cut_up_fasta.py), and the read coverage for these fragments was computed using
557 CONCOCT_coverage_table.py. The fragment coverages were then utilized for binning the 10 kb
558 fragments, and the clustered fragments underwent merging (merge_cutup_clustering.py) to
559 generate the final CONCOCT bins (extra_fasta_bins.py). To dereplicate and consolidate the
560 produced outputs from CONCOCT and MetaBAT2 binners, the metaWRAP (v1.2.3)[96] 'bin
561 refinement' command was employed, utilizing parameters '-x 10 -c 50'. These parameters signify
562 a maximum bin contamination threshold of 10% and a minimum bin completeness threshold of
563 50%, as determined by CheckM[97] estimates. Taxonomic annotation of generated bins was
564 performed using GTDB-Tk (v2.3.2)[98] command 'gtdbtk classify_wf' with default settings. Finally,
565 the abundances of the draft genomes (bins) across the samples were quantified using the
566 metaWRAP 'quant_bins' module.
567

568 To improve the consistency and quality of models representing the same species across different
569 samples, the bins for each common species (species that are not unique to one sample) were
570 reassembled by pooling the reads corresponding to that species from all samples. These
571 reassembled bins were then re-binned using the previously described procedure to generate a single
572 MAG per species (**Figure S3A;Table S5**). The only exception was a pooled *E. coli* MAG that was
573 8.2Mb in size, which exceeds the typical size range for *E. coli* genomes, suggesting it was likely
574 an artifact resulting from strain heterogeneity. To represent the multiple *E. coli* strains present
575 across samples without retaining the 23 sample-specific *E. coli* individual assemblies with varying

576 size and completeness, the bins derived from the individual assemblies were clustered based on
577 average nucleotide identity using the fastANI software[99]. A distance matrix was constructed, and
578 the bins were then clustered using the *hclust* function from the R-package stats. Five clusters were
579 selected, and five cluster-specific *E. coli* strains were re-assembled, each representing a species
580 pooled from samples within the corresponding cluster, followed by re-binning as described earlier.
581 The resulting 5 MAGs vary in size from 4 to 5.8 Mb which is within the expected range for the *E.*
582 *coli* genome[100] (**Figure S3A**).
583
584 As a result of applying these steps to the co-assembly of all samples, we found that only five
585 species had MAGs from the co-assembly that were of higher quality - based on completeness,
586 contamination, and N50 metrics - than those obtained from the pooled or single-sample assemblies.
587 These species were *Bacteroides fragilis*, *Anaerostipes butyraticus*, *Alistipes excrementavium*,
588 *Limihabitans stercoravium*, and *Caccovivens* s*p944345705*. Consequently, for these five species,
589 the representative MAG was selected from the co-assembly. The characteristics and classification
590 of the 237 reconstructed MAGs are provided in the **Table S5**.

591 **Model reconstruction and curation**

592 The MAGs with a minimum relative abundance of 0.5% in each sample underwent reconstruction
593 using gapseq v1.2 (commit 3e2d9393, Sequence DB md5sum: 17e92c9) with default settings[101],
594 resulting in a total of 233 metabolic models. Each sample was represented by 5 to 33 unique
595 MAGs. Since the specific dietary composition used as chicken feed was not disclosed in the
596 original study, the nutritional input for the models was formulated based on a typical chicken corn-
597 based diet[102] by translating molecular constituents into corresponding metabolites using vmh.org,
598 foodb.ca and feedtables.com resources[103–105]. Due to limited information on fiber in the chicken
599 diet, cellulose was utilized as a primary source of fibre according to available literature[106,107]. The
600 absorption and digestion of metabolites in the upper gut compartments were taken into account
601 when calculating the dietary input based on available information from studies on dietary
602 absorption in poultry gut[108–113]. Additionally, urea and mucus were introduced to depict the cecal
603 intestinal setting. Subsequently, this resulting nutritional composition served as an input medium
604 for gapfilling step via gapseq. To ensure microbial degradation capabilities towards dietary
605 components, profiling of carbohydrate-active enzymes (CAZymes) encoded within metagenomes

606 used for model reconstruction was performed using dbCAN3 tool[114], which is established upon
607 CAZy database - an expert-curated and routinely updated resource. Predicted CAZymes were
608 filtered by e-value threshold (> 1e-50) and required minimum 90% coverage with enzyme(s)
609 assigned EC number(s). Predicted EC numbers along with substrates were mapped to respective
610 reactions within modelSEED database and incorporated into models through gapseq adapt.
611 Additionally, metabolic models of the species known as SCFA producers, were examined on the
612 presence of fermentation pathways documented in the literature; missing pathways were added to
613 the models.

614 **Quantitative PCR**

615 qPCR of cecal digesta was performed using PercfeCTa SYBR green Supermix (Quantabio) with
616 Primers used target the universal 16S rRNA gene: Forward CGGYCCAGACTCCTACGGG,
617 Reverse TTACCGCGGCTGCTGGCAC[115]. The copy numbers were calculated back to copy
618 numbers per gram of cecal digesta.

619 **Set up of *in silico* ceca and simulation of sample-specific community models**

620 The microbial communities were simulated using the BacArena software[30], which combines Flux
621 Balance Analysis and individual-based modeling. BacArena represents each organism individually
622 on a two-dimensional grid to model a spatial environment. Metabolites can be exchanged between
623 individuals and diffuse in the environment, allowing for the dynamic update of the state of each
624 microbe and its surroundings. The initial microbial community was seeded on a 100x100 cell grid.
625 To mimic the flow of luminal contents in and out of the cecum while maintaining a relatively
626 stable bacterial population, the following approach was implemented. Multiple studies have shown
627 that the cecal contents are released only 2-3 times per day [116,117], which is a key feature for realistic
628 simulation, considering the cecum's role as a major hub for bacterial fermentation and SCFA
629 production.
630
631 At each hourly iteration, metabolites representing the metabolic contents from the upstream
632 compartment were added to the grid and evenly distributed between the grid cells, simulating
633 environmental mixing and allowing access to dietary and bacterial-derived metabolites to all cells
634 within the simulated environment. Every fourth iteration, a fraction of the cecum, including both

635 metabolites and microbes, was randomly removed to mimic emptying of the cecum. The number
636 of grid cells selected for removal of contents was determined to be 25% of the total to maintain
637 realistic fluctuations in bacterial density and a generally consistent community size. Low oxygen
638 concentrations (1e-08 mM) were to establish a nearly anaerobic environment reflective of reported
639 conditions in chicken ceca, along with pH of 7[118,119].
640
641 The absolute abundances of microbial communities were measured via quantitative PCR (qPCR)
642 assay, yielding copy numbers per gram of digesta ranging from 1.62e+09 to 3.02e+11. To reduce
643 skewness and ensure smaller values were distinguishable while preventing larger values from
644 dominating, we log-transformed these abundance values. Next, the log-transformed values were
645 rescaled to fit between 1000 and 5000. These rescaled values were then used as the total
646 abundances for the microbial communities in each sample. This approach ensured that even
647 species with low abundances were represented by at least 5 individuals on the grid, while also
648 allowing space for the community to grow and move within a grid of 10,000 cells. The
649 communities were simulated in 5 replicates during 16 iterations, each representing an hour, to
650 mimic the day of feeding.

651 **Comparison of functional capacities of community models**

652 Sets of unique reactions and pathways within each sample-specific microbiome were extracted
653 from the corresponding metabolic models comprising the sample. Binary matrices indicating the
654 presence or absence of reactions and pathways in each sample were created for subsequent Jaccard
655 distance calculations. Additionally, to quantify the metabolic potential within each sample while
656 accounting for the varying contributions of different species, we summarized the reaction and
657 pathway counts within each sample. Each reaction or pathway count was weighted by the relative
658 abundance of the species contributing to that reaction or pathway. The resulting incidence matrices
659 provided detailed information on the pathway and reaction abundance in the samples. Dissimilarity
660 matrices were constructed from the incidence matrices described using *vegdist* function from the
661 vegan R-package, and Principal Coordinate Analysis was performed using *cmdscale* function from
662 stats R-package. The network showcasing functional similarity between sample-specific
663 microbiomes was constructed using mutual information score calculated via *mutinformation*
664 function from infotheo R-package based on the metabolic reaction content of the samples. This

665 network was visualized using Cytoscape v.3.10.3[120], where large nodes represent samples, with
666 their sizes corresponding to the number of unique reactions in each sample. The smaller nodes
667 within a sample, representing taxonomic families, have sizes corresponding to the number of
668 reactions covered by the metabolic models of the species belonging to the respective taxonomic
669 families.
670
671 Community metabolic dissimilarity (CMD) score was calculated as the average of pairwise
672 metabolic dissimilarities based on EC numbers within the community, adjusted for the community
673 size. Specifically, the Bray-Curtis dissimilarity matrix for a sample was calculated from a
674 presence/absence matrix where the columns represent species and the rows represent EC numbers,
675 using the vegdist function from the vegan R-package. CMD score was then computed as a mean
676 of the dissimilarity matrix, with further log-adjustment to account for the diminishing contribution
677 of additional species in larger communities.

678 **Evaluation of cross-feeding and competition in *in silico* microbiomes**

679 To evaluate the extent of metabolic competition within Bacteroides-rich and Bacteroides-depleted
680 microbial communities, the metabolic resource overlap (MRO) between species was quantified
681 using the approach described in the original study[41]. The metabolic resource overlap (MRO) is a
682 metric that estimates the extent of overlap between the growth requirements of two or more
683 metabolic models[41]. As such, it quantifies the potential for species to compete for a predetermined
684 set of compounds in the media.
685
686 Cross-feeding interactions within microbial communities were investigated using metabolic
687 reaction fluxes. We filtered negligible fluxes to retain absolute total flux values above 1e-06
688 millimoles per hour per gram of dry weight (mmol/gDW/hour) and categorized species as
689 metabolite producers or consumers. By merging producer and consumer datasets on shared
690 metabolites, cross-feeding interactions were summarized by counting and normalizing interaction
691 occurrences across replicates within each category (based on *Bacteroides* presence). Key cross-
692 feeders were identified using a threshold of at least 10 interactions involving the exchange of 12
693 or more distinct metabolites, focusing on species with substantial and consistent metabolic activity.
694 Cross-feeding was quantified by retrieving all metabolite exchanges (import and export fluxes)

695 during simulations and calculating the number of total interactions (cross-feeding pairs) in each
696 sample. A cross-feeding coefficient was introduced as a metric of cross-feeding activity within a
697 community, defined as the number of total cross-feeding pairs formed divided by all possible
698 combinations of species pairs in the community. Interaction data were visualized using
699 ComplexHeatmap R-package.
700
701 Next, the total production and consumption for each metabolite was calculated over the course of
702 the simulation. The contribution of each species to the production and consumption was
703 determined as a percentage of the total production/consumption. Exchanged metabolites were
704 filtered to include only non-dietary metabolites, which are exclusively produced by bacteria. The
705 pairwise interactions involving non-dietary metabolites summarized across samples are visualized
706 as a heatmap in **Figure S6A** with raw data used to plot heatmap provided in **Table S3**.
707
708 To focus on metabolic niche adjustments involving keystone taxa, metabolites were further filtered
709 based on the following criteria: 1) they are predominantly produced or consumed by keystone taxa,
710 defined as those where at least 30% of produced metabolite is attributed to the production or
711 consumption by a single keystone taxon; 2) to ensure the metabolite is involved in cross-feeding,
712 at least 1% of the produced amount must be consumed by other species; 3) metabolites with the
713 same top producer (taxon that produces the highest amount of the metabolite) in both HB and NB
714 communities were excluded to emphasize shifts in metabolic roles. This filtering process resulted
715 in the identification of 22 key cross-fed metabolites. Of these, 18 were selected for downstream
716 visualization. Simple sugars D-Gluconate, D-Ribose, and D-Arabinose were excluded due to a
717 very low production levels, and L-Lactate was excluded because its production and consumption
718 patterns significantly overlapped with those of D-Lactate, so only D-Lactate is shown. For each
719 key cross-fed metabolite, the top three producers and consumers were identified based on their
720 relative contributions. The flux data was then subset to include only these key producer and
721 consumer species. Sankey diagrams were generated using the networkD3 R-package. To highlight
722 major contributors, a minimum contribution threshold of 5% was used for species shown in **Figure**
723 **5**.
724

To investigate differences in metabolite production and consumption between HB and NB microbial communities, the fluxes of exchanged metabolites were summarized within each community at every hour of the simulation and normalized by the total community size at that time point. Subsequently, the community fluxes (normalized by abundance) were aggregated over the 16-hour simulation period, and differences between the categories were evaluated using the Wilcoxon rank-sum statistical test. For graphical representation, metabolic fluxes were log2-transformed.

Statistical analyses

All statistical analyses were performed in R v4.2.3. Significant differences for numbers of reactions and pathways, metabolite concentrations, metabolic fluxes, community metabolic diversity and cross-feeding activity coefficients were determined by non-parametric Mann–Whitney U-test (Wilcoxon rank-sum test). Spearman's rank correlation coefficients and associated p-values were calculated between measured and predicted SCFA concentrations. Given *E. coli*'s high degree of connectivity, we explored its influence on metabolic exchanges within microbial communities. To evaluate how the presence or absence of this pivotal taxon determines the degree of cross-feeding activity, we constructed a linear model incorporating community size and the abundance of *E. coli* alongside key metabolic hubs: *A. butyraticus, L. crispatus,* and *B. fragilis* using the *lm* function in R. The response variable was the cross-feeding coefficient (CrossFeeding_coef), which quantifies the degree of metabolic interactions within the community. Predictor variables included categorical levels of *E. coli* abundance (Ecoli_category: "NoEcoli", "LowEcoli" (<5% relative abundance), "HighEcoli" (>5% relative abundance)), *Bacteroides* presence or absence that defines the community category (Bacteroides_presence: "NB" or "HB"), the presence of key taxa such as *Anaerostipes butyraticus* (Abutyraticus_presence) and *Lactobacillus crispatus* (Lcrispatus_presence), and community size (comm_size). Interaction terms between *E. coli* abundance and the other predictors were included to capture potential synergistic or antagonistic effects on cross-feeding. The model was specified as follows: *'CrossFeeding_coef ~ Ecoli_category:(Bacteroides_presence + Abutyraticus_presence + Lcrispatus_presence) + comm_size'*. The model summary is provided in the **Table S3**. All statistical analyses employed a significance threshold of p-value < 0.05.

FUNDING SOURCES

This work was funded by grants from the Natural Sciences and Engineering Research Council of Canada (RGPIN-2019-06852) and the Ontario Research Fund-Research Excellence. High performance computing was provided by the SciNet HPC Consortium. SciNet is funded by Innovation, Science and Economic Development Canada; the Digital Research Alliance of Canada; the Ontario Research Fund: Research Excellence; and the University of Toronto. The funders had no role in study design, data collection and analysis, decision to publish, or preparation of the manuscript.

AUTHOR CONTRIBUTIONS

J.P. and I.U. conceived and designed the study. I.U. performed simulations and data analysis. Y.F. performed qPCR experiments. B.P.W. provided critical reagents and contributed to data analysis. J.P. and I.U wrote the manuscript. All authors reviewed and/or edited the manuscript.

COMPETING INTERESTS

The authors declare no competing interests.

DATA AVAILABILITY STATEMENT

Microbial metabolic models and the source code used for simulations and data analysis have been deposited on GitHub (github.com/ParkinsonLab/Chicken_microbiome).

REFERENCES

1. Culp, E. J. & Goodman, A. L. Cross-feeding in the gut microbiome: Ecology and mechanisms. *Cell Host and Microbe* vol. 31 Preprint at https://doi.org/10.1016/j.chom.2023.03.016 (2023).
2. Gibbons, S. M. Keystone taxa indispensable for microbiome recovery. *Nature Microbiology* vol. 5 Preprint at https://doi.org/10.1038/s41564-020-0783-0 (2020).
3. Banerjee, S., Schlaeppi, K. & van der Heijden, M. G. A. Keystone taxa as drivers of microbiome structure and functioning. *Nature Reviews Microbiology* vol. 16 Preprint at https://doi.org/10.1038/s41579-018-0024-1 (2018).

786 4. Herren, C. M. & McMahon, K. D. Keystone taxa predict compositional change in microbial
787 communities. *Environ Microbiol* **20**, (2018).
788 5. Garrett, W. S. *et al.* Enterobacteriaceae Act in concert with the gut microbiota to induce
789 spontaneous and maternally transmitted colitis. *Cell Host Microbe* **8**, (2010).
790 6. Hajishengallis, G. *et al.* Low-abundance biofilm species orchestrates inflammatory
791 periodontal disease through the commensal microbiota and complement. *Cell Host Microbe*
792 **10**, (2011).
793 7. Banerjee, S. *et al.* Network analysis reveals functional redundancy and keystone taxa
794 amongst bacterial and fungal communities during organic matter decomposition in an arable
795 soil. *Soil Biol Biochem* **97**, (2016).
796 8. Lan, P. T. N., Hayashi, H., Sakamoto, M. & Benno, Y. Phylogenetic analysis of cecal
797 microbiota in chicken by the use of 16S rDNA clone libraries. *Microbiol Immunol* **46**,
798 (2002).
799 9. Qi, Z., Shi, S., Tu, J. & Li, S. Comparative metagenomic sequencing analysis of cecum
800 microbiotal diversity and function in broilers and layers. *3 Biotech* **9**, (2019).
801 10. Oakley, B. B. *et al.* Successional changes in the chicken cecal microbiome during 42 days
802 of growth are independent of organic acid feed additives. *BMC Vet Res* **10**, 1–8 (2014).
803 11. Fan, Y., Ju, T., Bhardwaj, T., Korver, D. R. & Willing, B. P. Week-Old Chicks with High
804 Bacteroides Abundance Have Increased Short-Chain Fatty Acids and Reduced Markers of
805 Gut Inflammation . *Microbiol Spectr* **11**, (2023).
806 12. Zou, A., Sharif, S. & Parkinson, J. Lactobacillus elicits a ' Marmite effect ' on the chicken
807 cecal microbiome. *NPJ Biofilms Microbiomes* **4**, 1–5 (2018).
808 13. Melkonian, C. *et al.* Microbial interactions shape cheese flavour formation. *Nat Commun*
809 **14**, (2023).
810 14. Giordano, N. *et al.* Genome-scale community modelling reveals conserved metabolic cross-
811 feedings in epipelagic bacterioplankton communities. *Nat Commun* **15**, 2721 (2024).
812 15. Zampieri, G., Campanaro, S., Angione, C. & Treu, L. Metatranscriptomics-guided genome-
813 scale metabolic modeling of microbial communities. *Cell Reports Methods* **3**, (2023).
814 16. Quinn-Bohmann, N. *et al.* Microbial community-scale metabolic modelling predicts
815 personalized short-chain fatty acid production profiles in the human gut. *Nat Microbiol* **9**,
816 1700–1712 (2024).

817 17. Bauer, E. & Thiele, I. From metagenomic data to personalized in silico microbiotas :
818 predicting dietary supplements for Crohn ' s disease. *NPJ Syst Biol Appl* **4**, (2018).
819 18. Marcelino, V. R. *et al.* Disease-specific loss of microbial cross-feeding interactions in the
820 human gut. *Nat Commun* **14**, (2023).
821 19. Heinken, A., Hertel, J. & Thiele, I. Metabolic modelling reveals broad changes in gut
822 microbial metabolism in inflammatory bowel disease patients with dysbiosis. *NPJ Syst Biol*
823 *Appl* **7**, (2021).
824 20. Kumar, S. *et al.* Effect of antibiotic withdrawal in feed on chicken gut microbial dynamics
825 , immunity , growth performance and prevalence of foodborne pathogens. *PLoS One* **13**, 1–
826 23 (2018).
827 21. Caspi, R. *et al.* The MetaCyc database of metabolic pathways and enzymes and the BioCyc
828 collection of pathway/genome databases. *Nucleic Acids Res* **44**, (2016).
829 22. Humbel, F. *et al.* Association of Alterations in Intestinal Microbiota With Impaired
830 Psychological Function in Patients With Inflammatory Bowel Diseases in Remission.
831 *Clinical Gastroenterology and Hepatology* **18**, (2020).
832 23. Bowerman, K. L. *et al.* Disease-associated gut microbiome and metabolome changes in
833 patients with chronic obstructive pulmonary disease. *Nat Commun* **11**, (2020).
834 24. Crossfield, M. *et al.* Archaeal and Bacterial Metagenome-Assembled Genome Sequences
835 Derived from Pig Feces. *Microbiol Resour Announc* **11**, (2022).
836 25. Gilroy, R. *et al.* Metagenomic investigation of the equine faecal microbiome reveals
837 extensive taxonomic diversity. *PeerJ* **10**, (2022).
838 26. Zhang, X.-X. *et al.* A Catalog of over 5,000 Metagenome-Assembled Microbial Genomes
839 from the Caprinae Gut Microbiota. *Microbiol Spectr* **10**, (2022).
840 27. Gilroy, R. *et al.* Extensive microbial diversity within the chicken gut microbiome revealed
841 by metagenomics and culture. *PeerJ* **9**, (2021).
842 28. Nayfach, S., Shi, Z. J., Seshadri, R., Pollard, K. S. & Kyrpides, N. C. New insights from
843 uncultivated genomes of the global human gut microbiome. *Nature* **568**, (2019).
844 29. Wang, Y. *et al.* Phylogenomics of expanding uncultured environmental Tenericutes
845 provides insights into their pathogenicity and evolutionary relationship with Bacilli. *BMC*
846 *Genomics* **21**, (2020).

847 30. Bauer, E., Zimmermann, J., Baldini, F., Thiele, I. & Kaleta, C. BacArena: Individual-based
848 metabolic modeling of heterogeneous microbes in complex communities. *PLoS Comput*
849 *Biol* **13**, (2017).
850 31. Salvi, P. S. & Cowles, R. A. Butyrate and the intestinal epithelium: Modulation of
851 proliferation and inflammation in homeostasis and disease. *Cells* vol. 10 Preprint at
852 https://doi.org/10.3390/cells10071775 (2021).
853 32. Van Immerseel, F. *et al.* Interactions of butyric acid- and acetic acid-treated Salmonella
854 with chicken primary cecal epithelial cells in vitro. *Avian Dis* **48**, (2004).
855 33. Rios-Covian, D., Gueimonde, M., Duncan, S. H., Flint, H. J. & De Los Reyes-Gavilan, C.
856 G. Enhanced butyrate formation by cross-feeding between Faecalibacterium prausnitzii and
857 Bifidobacterium adolescentis. *FEMS Microbiol Lett* **362**, (2015).
858 34. Reichardt, N. *et al.* Phylogenetic distribution of three pathways for propionate production
859 within the human gut microbiota. *ISME Journal* **8**, (2014).
860 35. Geirnaert, A. *et al.* Butyricicoccus pullicaecorum, a butyrate producer with probiotic
861 potential, is intrinsically tolerant to stomach and small intestine conditions. *Anaerobe* **30**,
862 (2014).
863 36. Louis, P. & Flint, H. J. Diversity, metabolism and microbial ecology of butyrate-producing
864 bacteria from the human large intestine. *FEMS Microbiol Lett* **294**, (2009).
865 37. Feng, J. *et al.* Polysaccharide utilization loci in Bacteroides determine population fitness
866 and community-level interactions. *Cell Host Microbe* **30**, (2022).
867 38. Liu, H. *et al.* Ecological dynamics of the gut microbiome in response to dietary fiber. *ISME*
868 *Journal* **16**, (2022).
869 39. Shin, J. H. *et al.* Bacteroides and related species: The keystone taxa of the human gut
870 microbiota. *Anaerobe* vol. 85 Preprint at https://doi.org/10.1016/j.anaerobe.2024.102819
871 (2024).
872 40. Weiss, A. S. *et al.* Nutritional and host environments determine community ecology and
873 keystone species in a synthetic gut bacterial community. *Nat Commun* **14**, (2023).
874 41. Zelezniak, A. *et al.* Metabolic dependencies drive species co-occurrence in diverse
875 microbial communities. *Proc Natl Acad Sci U S A* **112**, (2015).
876 42. Giri, S. *et al.* Metabolic dissimilarity determines the establishment of cross-feeding
877 interactions in bacteria. *Current Biology* **31**, (2021).

878 43. Krautkramer, K. A., Fan, J. & Bäckhed, F. Gut microbial metabolites as multi-kingdom
879 intermediates. *Nature Reviews Microbiology* vol. 19 Preprint at
880 https://doi.org/10.1038/s41579-020-0438-4 (2021).
881 44. Dabrock, B., Riedel, J., Bertram, J. & Gottschalk, G. Isopropylbenzene (cumene) - a new
882 substrate for the isolation of trichloroethene-degrading bacteria. *Arch Microbiol* **158**,
883 (1992).
884 45. Liu, C. J. *et al.* Complete genome sequences and comparative genome analysis of
885 Lactobacillus plantarum strain 5-2 isolated from fermented soybean. *Genomics* **106**, (2015).
886 46. Zhou, Y. & Zhi, F. Lower Level of Bacteroides in the Gut Microbiota Is Associated with
887 Inflammatory Bowel Disease: A Meta-Analysis. *BioMed Research International* vol. 2016
888 Preprint at https://doi.org/10.1155/2016/5828959 (2016).
889 47. Vich Vila, A. *et al.* Gut microbiota composition and functional changes in inflammatory
890 bowel disease and irritable bowel syndrome. *Sci Transl Med* **10**, (2018).
891 48. Xu, X. *et al.* The gut metagenomics and metabolomics signature in patients with
892 inflammatory bowel disease. *Gut Pathog* **14**, (2022).
893 49. Lloyd-Price, J. *et al.* Multi-omics of the gut microbial ecosystem in inflammatory bowel
894 diseases. *Nature* **569**, (2019).
895 50. Knights, D. *et al.* Complex host genetics influence the microbiome in inflammatory bowel
896 disease. *Genome Med* **6**, (2014).
897 51. Pascal, V. *et al.* A microbial signature for Crohn's disease. *Gut* **66**, (2017).
898 52. Willing, B. P. *et al.* A pyrosequencing study in twins shows that gastrointestinal microbial
899 profiles vary with inflammatory bowel disease phenotypes. *Gastroenterology* **139**, (2010).
900 53. Franzosa, E. A. *et al.* Gut microbiome structure and metabolic activity in inflammatory
901 bowel disease. *Nat Microbiol* **4**, (2019).
902 54. Hove, H. & Mortensen, P. B. Influence of intestinal inflammation (IBD) and small and large
903 bowel length on fecal short-chain fatty acids and lactate. *Dig Dis Sci* **40**, (1995).
904 55. Roediger, W. E. W. THE COLONIC EPITHELIUM IN ULCERATIVE COLITIS: AN
905 ENERGY-DEFICIENCY DISEASE? *The Lancet* **316**, (1980).
906 56. Kameyama, J. I., Narui, H., Inui, M. & Sato, T. Energy Level in Large Intestinal Mucosa in
907 Patients with Ulcerative Colitis. *Tohoku J Exp Med* **143**, (1984).

908 57. Bjerrum, J. T. *et al.* Metabonomics of human fecal extracts characterize ulcerative colitis,
909 Crohn's disease and healthy individuals. *Metabolomics* **11**, (2015).
910 58. Xu, H. M. *et al.* Characterization of short-chain fatty acids in patients with ulcerative colitis:
911 a meta-analysis. *BMC Gastroenterol* **22**, (2022).
912 59. Braun, T. *et al.* Diet-omics in the Study of Urban and Rural Crohn disease Evolution
913 (SOURCE) cohort. *Nat Commun* **15**, (2024).
914 60. Morgan, X. C. *et al.* Dysfunction of the intestinal microbiome in inflammatory bowel
915 disease and treatment. *Genome Biol* **13**, (2012).
916 61. Lewis, J. D. *et al.* Inflammation, Antibiotics, and Diet as Environmental Stressors of the
917 Gut Microbiome in Pediatric Crohn's Disease. *Cell Host Microbe* **18**, (2015).
918 62. Ellestad-Sayed, J. J., Nelson, R. A., Adson, M. A., Palmer, W. M. & Soule, E. H.
919 Pantothenic acid, coenzyme A, and human chronic ulcerative and granulomatous colitis.
920 *American Journal of Clinical Nutrition* **29**, (1976).
921 63. Veseli, I. *et al.* Microbes with higher metabolic independence are enriched in human gut
922 microbiomes under stress. *bioRxiv* (2023) doi:10.1101/2023.05.10.540289.
923 64. Bushman, F. D. *et al.* Multi-omic Analysis of the Interaction between Clostridioides
924 difficile Infection and Pediatric Inflammatory Bowel Disease. *Cell Host Microbe* **28**,
925 (2020).
926 65. Filippi, J., Al-Jaouni, R., Wiroth, J. B., Hébuterne, X. & Schneider, S. M. Nutritional
927 deficiencies in patients with Crohn's disease in remission. *Inflamm Bowel Dis* **12**, (2006).
928 66. Huang, Y. L., Chassard, C., Hausmann, M., Von Itzstein, M. & Hennet, T. Sialic acid
929 catabolism drives intestinal inflammation and microbial dysbiosis in mice. *Nat Commun* **6**,
930 (2015).
931 67. Liang, Q. *et al.* Sialic acid plays a pivotal role in licensing Citrobacter rodentium's transition
932 from the intestinal lumen to a mucosal adherent niche. *Proc Natl Acad Sci U S A* **120**,
933 (2023).
934 68. Xun, W. *et al.* Specialized metabolic functions of keystone taxa sustain soil microbiome
935 stability. *Microbiome* **9**, (2021).
936 69. Ze, X., Duncan, S. H., Louis, P. & Flint, H. J. Ruminococcus bromii is a keystone species
937 for the degradation of resistant starch in the human colon. *ISME Journal* **6**, (2012).

938 70. Trosvik, P. & de Muinck, E. J. Ecology of bacteria in the human gastrointestinal tract--
939 identification of keystone and foundation taxa. *Microbiome* **3**, (2015).
940 71. Cartmell, A. *et al.* A surface endogalactanase in Bacteroides thetaiotaomicron confers
941 keystone status for arabinogalactan degradation. *Nat Microbiol* **3**, (2018).
942 72. Fisher, C. K. & Mehta, P. Identifying keystone species in the human gut microbiome from
943 metagenomic timeseries using sparse linear regression. *PLoS One* **9**, (2014).
944 73. Rychlik, I. Composition and function of chicken gut microbiota. *Animals* **10**, (2020).
945 74. Mancabelli, L. *et al.* Insights into the biodiversity of the gut microbiota of broiler chickens.
946 *Environ Microbiol* **18**, (2016).
947 75. Marcolla, C. S., Ju, T., Lantz, H. L. & Willing, B. P. Investigating the cecal microbiota of
948 broilers raised in extensive and intensive production systems. *Microbiol Spectr* **11**, (2023).
949 76. Roberts, T. *et al.* New issues and science in broiler chicken intestinal health: Intestinal
950 microbial composition, shifts, and impacts. *Worlds Poult Sci J* **71**, (2015).
951 77. Huang, Y. *et al.* Community composition of cecal microbiota in commercial yellow broilers
952 with high and low feed efficiencies. *Poult Sci* **100**, (2021).
953 78. Chen, Y. *et al.* Chicken cecal microbiota reduces abdominal fat deposition by regulating fat
954 metabolism. *NPJ Biofilms Microbiomes* **9**, (2023).
955 79. Lo Sasso, G. *et al.* Inflammatory Bowel Disease-Associated Changes in the Gut: Focus on
956 Kazan Patients. *Inflamm Bowel Dis* **27**, (2021).
957 80. Zheng, L. & Wen, X. L. Gut microbiota and inflammatory bowel disease: The current status
958 and perspectives. *World J Clin Cases* **9**, (2021).
959 81. Midani, F. S. & David, L. A. Tracking defined microbial communities by multicolor flow
960 cytometry reveals tradeoffs between productivity and diversity. *Front Microbiol* **13**, (2023).
961 82. Goodman, A. L. *et al.* Identifying Genetic Determinants Needed to Establish a Human Gut
962 Symbiont in Its Habitat. *Cell Host Microbe* **6**, (2009).
963 83. Ray, K. J., Santee, C., McCauley, K., Panzer, A. R. & Lynch, S. V. Gut Bifidobacteria
964 enrichment following oral Lactobacillus-supplementation is associated with clinical
965 improvements in children with cystic fibrosis. *BMC Pulm Med* **22**, (2022).
966 84. Ma, C. *et al.* The gut microbiome stability is altered by probiotic ingestion and improved
967 by the continuous supplementation of galactooligosaccharide. *Gut Microbes* (2020)
968 doi:10.1080/19490976.2020.1785252.

969 85. Armougom, F., Henry, M., Vialettes, B., Raccah, D. & Raoult, D. Monitoring bacterial
970 community of human gut microbiota reveals an increase in Lactobacillus in obese patients
971 and Methanogens in anorexic patients. *PLoS One* **4**, (2009).
972 86. Nieuwdorp, M., Gilijamse, P. W., Pai, N. & Kaplan, L. M. Role of the microbiome in energy
973 regulation and metabolism. *Gastroenterology* **146**, (2014).
974 87. Fan, Y. & Pedersen, O. Gut microbiota in human metabolic health and disease. *Nature*
975 *Reviews Microbiology* vol. 19 Preprint at https://doi.org/10.1038/s41579-020-0433-9
976 (2021).
977 88. Diener, C. & Gibbons, S. M. More is Different: Metabolic Modeling of Diverse Microbial
978 Communities. *mSystems* **8**, (2023).
979 89. Bosi, E., Bacci, G., Mengoni, A. & Fondi, M. Perspectives and Challenges in Microbial
980 Communities Metabolic Modeling. **8**, 1–9 (2017).
981 90. Bushnell, B. BBTools. *DOE Joint Genome Institute* Preprint at (2014).
982 91. Li, D., Liu, C. M., Luo, R., Sadakane, K. & Lam, T. W. MEGAHIT: An ultra-fast single-
983 node solution for large and complex metagenomics assembly via succinct de Bruijn graph.
984 *Bioinformatics* **31**, (2015).
985 92. Langmead. Bowtie2. *Nat Methods* **9**, (2013).
986 93. Kang, D. D. *et al.* MetaBAT 2: An adaptive binning algorithm for robust and efficient
987 genome reconstruction from metagenome assemblies. *PeerJ* **2019**, (2019).
988 94. Alneberg, J. *et al.* Binning metagenomic contigs by coverage and composition. *Nat Methods*
989 **11**, (2014).
990 95. Li, H. *et al.* The Sequence Alignment/Map format and SAMtools. *Bioinformatics* **25**,
991 (2009).
992 96. Uritskiy, G. V., DiRuggiero, J. & Taylor, J. MetaWRAP—a flexible pipeline for genome-
993 resolved metagenomic data analysis. *Microbiome* **6**, (2018).
994 97. Parks, D. H., Imelfort, M., Skennerton, C. T., Hugenholtz, P. & Tyson, G. W. CheckM:
995 Assessing the quality of microbial genomes recovered from isolates, single cells, and
996 metagenomes. *Genome Res* **25**, (2015).
997 98. Chaumeil, P. A., Mussig, A. J., Hugenholtz, P. & Parks, D. H. GTDB-Tk v2: memory
998 friendly classification with the genome taxonomy database. *Bioinformatics* **38**, (2022).

999 99. Jain, C., Rodriguez-R, L. M., Phillippy, A. M., Konstantinidis, K. T. & Aluru, S. High
1000 throughput ANI analysis of 90K prokaryotic genomes reveals clear species boundaries. *Nat*
1001 *Commun* **9**, (2018).
1002 100. Abram, K. *et al.* Mash-based analyses of Escherichia coli genomes reveal 14 distinct
1003 phylogroups. *Commun Biol* **4**, (2021).
1004 101. Zimmermann, J., Kaleta, C. & Waschina, S. gapseq: informed prediction of bacterial
1005 metabolic pathways and reconstruction of accurate metabolic models. *Genome Biol* **22**,
1006 (2021).
1007 102. Zou, A. *et al.* Systematic profiling of the chicken gut microbiome reveals dietary
1008 supplementation with antibiotics alters expression of multiple microbial pathways with
1009 minimal impact on community structure. *Microbiome* **10**, (2022).
1010 103. Noronha, A. *et al.* The Virtual Metabolic Human database : integrating human and gut
1011 microbiome metabolism with nutrition and disease. *Nucleic Acids Res* **47**, 614–624 (2018).
1012 104. www.foodb.ca.
1013 105. AFZ. INRA-CIRAD-AFZ feed tables: composition and nutritive values of feeds for cattle,
1014 sheep, goats, pigs, poultry, rabbits, horses, and salmonids. Feedtables.com, INRAE,
1015 CIRAD, AFZ. (2017).
1016 106. Tejeda, O. J. & Kim, W. K. Role of dietary fiber in poultry nutrition. *Animals* vol. 11
1017 Preprint at https://doi.org/10.3390/ani11020461 (2021).
1018 107. Erik, K. & Knudsen, B. Fiber and nonstarch polysaccharide content and variation in
1019 common crops used in broiler diets 1. 2380–2393 (2012).
1020 108. Riesenfeld, G., Sklan, D., Bar, A., Eisner, U. & Hurwitz, S. Glucose absorption and starch
1021 digestion in the intestine of the chicken. *Journal of Nutrition* **110**, 117–121 (1980).
1022 109. Khalil, M. M., Abdollahi, M. R., Zaefarian, F. & Ravindran, V. Measurement of ileal
1023 endogenous energy losses and true ileal digestible energy of cereal grains for broiler
1024 chickens. *Poult Sci* **99**, (2020).
1025 110. Bielorai, R. & Iosif, B. Amino acid absorption and endogenous amino acids in the lower
1026 ileum and excreta of chicks. *Journal of Nutrition* **117**, 1459–1462 (1987).
1027 111. Bielorai, R., Tamir, M. & Hurwitz, S. Amino acid absorption along the intestinal tract of
1028 chicks fed heated and raw soybean meal. *Journal of Nutrition* **107**, 1775–1778 (1977).

1029 112. Tancharoenrat, P., Ravindran, V., Zaefarian, F. & Ravindran, G. Digestion of fat and fatty
1030 acids along the gastrointestinal tract of broiler chickens. *Poult Sci* **93**, 371–379 (2014).
1031 113. Rodriguez-Sanchez, R., Tres, A., Sala, R., Guardiola, F. & Barroeta, A. C. Evolution of
1032 lipid classes and fatty acid digestibility along the gastrointestinal tract of broiler chickens
1033 fed different fat sources at different ages. *Poult Sci* **98**, 1341–1353 (2019).
1034 114. Zheng, J. *et al.* DbCAN3: Automated carbohydrate-Active enzyme and substrate
1035 annotation. *Nucleic Acids Res* **51**, (2023).
1036 115. Forgie, A. J. *et al.* Pea polyphenolics and hydrolysis processing alter microbial community
1037 structure and early pathogen colonization in mice. *Journal of Nutritional Biochemistry* **67**,
1038 (2019).
1039 116. Duke, G. E., Eccleston, E., Louis, C. F. & Bedbury, H. P. Cellulose digestion by domestic
1040 turkeys fed low or high fiber diets. *Journal of Nutrition* **114**, 95–102 (1984).
1041 117. Duke, G. E. Relationship of cecal and colonic motility to diet, habitat, and cecal anatomy
1042 in several avian species. *Journal of Experimental Zoology* **252**, 38–47 (1989).
1043 118. Ravindran, V. Feed enzymes: The science, practice, and metabolic realities. *Journal of*
1044 *Applied Poultry Research* **22**, 628–636 (2013).
1045 119. Nguyen, H. T., Bedford, M. R., Wu, S. B. & Morgan, N. K. Soluble non-starch
1046 polysaccharide modulates broiler gastrointestinal tract environment. *Poult Sci* **100**, (2021).
1047 120. Su, G., Morris, J. H., Demchak, B. & Bader, G. D. Biological Network Exploration with
1048 Cytoscape 3. *Curr Protoc Bioinformatics* **2014**, (2014).
1049
1050

1051
1052

1053
1054
1055
1056